Theoretical and Applied Fracture Mechanics 133 (2024) 104476

Contents lists available at ScienceDirect

Theoretical and Applied Fracture Mechanics

journal homepage: www.elsevier.com/locate/tafmec

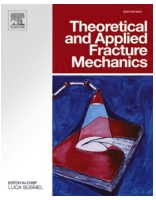

Experimental studies on the static sharp notch effects during dynamic crack kinking/nucleation at the material interfaces

Luoyu Roy Xu

School of Mechanical Engineering and Mechanics, Ningbo University, Zhejiang Province 315000, China

ARTICLE INFO

Keywords:
Crack kinking
Interface
Notch
Stress singularity

ABSTRACT

Dynamic fracture experiments on four bonded polymers using high-speed photography showed that different static sharp notches formed after the incident dynamic cracks met the material interfaces. In one scenario, an incident dynamic crack induced interfacial crack nucleation, and two convex notches formed after the interfacial crack propagated away. In another scenario, interface-induced crack kinking and a "head-to-tail" crack kinking pattern led to a concave notch with a singular stress field, which merits consideration in fracture mechanics modeling. In contrast, load-induced crack kinking did not cause the above scenarios. In another unique experimental phenomenon, a slightly curved/kinked dynamic crack only had a small local crack kinking angle, but its final crack direction was almost 90° to the initial crack direction over a long crack path.

1. Introduction

Dynamic failure and crack propagation has been a long-standing research topic [19,32,11,12,29,13,3,23,31,21,28,38,1,43,7,47,6] (Kistler and Waas, 1998). As shown in Fig. 1, when two dynamic cracks encounter the same material interface, three dynamic failure modes, crack penetration, load-induced crack kinking, and interface-induced crack kinking, often occur. Either the incident crack penetrates the interface and continues to propagate, which is referred to as crack penetration [16,15], or the incident crack kinks into the interface, which is referred to as crack kinking or deflection [42,17,49,35]. There are two kinds of crack kinking due to different mechanisms. The applied load or local load mixity variations can lead to dynamic crack kinking or load-induced crack kinking, as shown in Fig. 1. Usually, the crack path is quite smooth. Simultaneously, if there is a significant reducation in the fracture toughness of the interface over the bulk material, an incident crack may kink into the interface and leave a sharp concave notch, which is referred to as interface-induced crack kinking. In previous crack kinking studies, the sharp notch was almost always disregarded. However, with the extensive application of composite and layered materials, investigation of material interface failure has become vital [20,41]. Hence, the interface-induced crack kinking phenomenon merits greater attention, especially in 3D printing materials, which are typical layered materials with numerous interfaces.

Immediately after the 3D polymer printing technique was first introduced in 1986, Knauss and a co-worker conducted pioneering research on dynamic crack propagation along an interface [22]. They employed weakly bonded polymers (Plexiglass or PMMA and Homalite) to measure the mode-I dynamic crack speed along the interface. Later, Rosakis et al. studied interfacial shear cracks and mixed-mode cracks using bonded polymers [34,46]. As illustrated in Figs. 1 and 2, these polymer specimens were bonded together using selected adhesives to form artificial interfaces. Because the mechanical properties, such as the Young's moduli, of these special adhesives after curing are similar to those of bulk polymers, the adhesives are considered bulk polymer components. Therefore, the bonded materials can be treated as homogeneous and isotropic materials except at their interfaces, which usually have lower strength or toughness than the bulk polymers. Fig. 2(a) shows a layered Homalite plate with two bonded interfaces after a projectile impact at the bottom layer. Fig. 2(b) shows a cross-sectional view of a 3D printing polymer [4]. These two kinds of layered materials are the same with regard to the mechanical features. They are homogeneous and isotropic in terms of stiffness and wave propagations, but anisotropic in terms of their strengths or fracture toughnesses due to these interfaces. Therefore, the bonded polymers in Fig. 2(a) can be viewed as "model 3D printing materials".

As the structural applications of 3D printing materials have rapidly increased, crack propagation and interaction with numerous interfaces have become a critical safety topic, especially considering the absence of systematic studies such as on complicated crack propagations of mode-II and mixed-mode cracks. Hence, in this study, we focused on sharp notches related to interfaces.

E-mail address: l.roy.xu@alumni.caltech.edu.

https://doi.org/10.1016/j.tafmec.2024.104476
Received 27 November 2023; Received in revised form 6 April 2024; Accepted 15 May 2024
Available online 18 May 2024

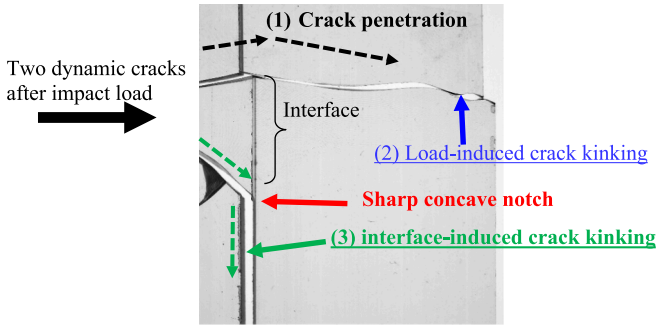

Fig. 1. Impacted Homalite polymer plate with three dynamic failure modes: (1) Dynamic crack penetration across an interface, (2) Load-induced crack kinking, and (3) Interface-induced crack kinking. A sharp concave notch forms between the incident crack and the kinked interface crack.

2. Theoretical background

2.1. Stress and stress intensity factors before and after crack kinking

We employed static crack kinking theory to obtain an initial understanding of a complicated dynamic fracture problem, especially the sharp notches that were static with respect to the dynamic cracks. Based on linear elastic fracture mechanics, the two-dimensional full-field stress of a mixed-mode crack, as seen in Fig. 3, can be expressed in a polar coordinate system [5,48]:

$$\sigma_{ij}(r,\theta)=\frac{K_I}{\sqrt{2\pi r}}\sum_{ij}^{I}(\theta)+T\delta_{i1}\delta_{j1}+\frac{K_{II}}{\sqrt{2\pi r}}\sum_{ij}^{II}(\theta)+O(r^{\frac{1}{2}})\quad(i,j=1,2), \tag{1}$$

where K_I and K_{II} are the static mode I and mode II stress intensity factors, respectively. According to dynamic fracture mechanics theory [11], the dynamic stress intensity factors are functions of the static stress intensity factors and crack tip speeds. Assuming that all crack speeds are small, the dynamic stress intensity factors are close to the static stress intensity factors. T is a nonsingular stress term, $O(r^{\frac{1}{2}})$ represents higher-order terms of the length scale r and is dropped if the kinked crack length "l" is very small, and the known functions $\Sigma_{ij}^{I}(\theta),\Sigma_{ij}^{II}(\theta)$ represent the angular variations of the 2-D stress components.

Previous research on crack kinking has mainly focused on the relation between the stress intensity factors before and after crack kinking based on one key assumption; that is, the head of the main crack immediately became the tail of the kinked crack. Therefore, the asymptotic stress fields before and after crack kinking were assumed to be the same, and some simplified relations among the static stress intensity factors were obtained (Contrell and Rice, 1980):

$$\sigma_{ij}^{kc}=\sigma_{ij}^{mc}\quad if\ \ l\ \ and\ \ r\to 0,\quad (i,j=1,2), \tag{2}$$

$$\begin{aligned}k_I^{kc}&=c_{11}K_I^{mc}+c_{12}K_{II}^{mc},\\ k_{II}^{kc}&=c_{21}K_I^{mc}+c_{22}K_{II}^{mc}.\end{aligned} \tag{3}$$

where "mc" and "kc" denote "main crack" and "kinked crack." The coefficients c_{ij} $(i,j=1,2)$ were reported by Contrell and Rice [8]. To include the role of the T-stress, Li and Xu [26] derived new relationships among the stress intensity factors and the T-stresses for different static crack kinking cases. Although complicated dynamic crack penetration and kinking modeling results at interfaces are available [46,14], we do not cite these results here to simplify a complicated fracture problem.

2.2. Singular stress field of a sharp concave notch

As shown in Fig. 3(b), a sharp concave notch formed immediately after crack kinking. Its asymptotic stress field can be described by two generalized stress intensity factors, $K_I^{notch},K_{II}^{notch}$ based on Williams' pioneering work (1952):

$$\sigma_{ij}^{notch}(r,\theta)=K_I^{notch}r^{\lambda-1}f_{ij}(\theta)+K_{II}^{notch}r^{\xi-1}g_{ij}(\theta)\ \ r\to 0\quad(i,j=1,2), \tag{4}$$

where the known functions $f_{ij}(\theta),g_{ij}(\theta)$ represent the angular variations related to the mode-I and mode-II stresses, and (λ-1) and (ξ-1) are the mode-I and mode-II stress singular orders, which are mainly determined by the notch angle $(180^\circ-\beta)$, as shown in Fig. 3. If the notch angle is less than 180°, the stress is singular at the concave notch tip [36].

2.3. Caustic at a crack or a notch tip

In dynamic fracture experiments, as shown in Fig. 3, a black spot (caustic) is often observed at the crack tip (especially the mode-I crack tip of a transparent material). Because of the high tensile stress at the crack tip, the through-thickness deformation is large. Therefore, incident light rays are deflected, and some rays cannot reach the film plane of the camera, so a black spot forms in the photo. Extensive research has shown that the diameter of a caustic at a crack tip is an increasing function of the stress intensity factor [33] (Gdoutos, 2016). Similarly, a notch may have a caustic if its mode-I generalized stress intensity factor is large. Notably, the purpose of this experimental investigation was to discover unique phenomena that merit the attention of theoreticians. For example, Contrell and Rice [8] only modeled a slightly curved crack, rather than a complicated kinked crack with a sharp notch. As this was an experimental study, the challenging modeling or simulation work would be outside the scope of this paper.

3. Experimental investigation

Two types of polymeric materials were employed in conjunction with two kinds of optical diagnostic techniques. Homalite-100 was chosen for the dynamic photoelasticity experiments, whereas Plexiglas (PMMA) was used in the Coherent Gradient Sensing (CGS) experiments [30]. Tables 1 and 2 show selected material properties of Homalite and PMMA. Dynamic photoelasticity was used to record the maximum in-plane shear stresses (fringes) in a specimen during the loading

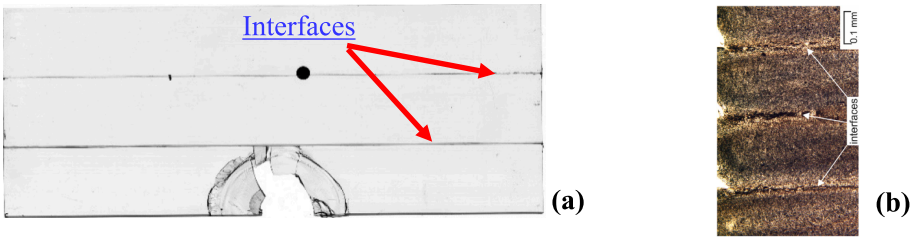

Fig. 2. (a) Layered Homalite plate with two bonded interfaces after a projectile impact, (b) Cross-sectional view of a 3D printing polylactide (PLA) specimen with three interfaces [4]. The layer thicknesses of (a) and (b) are 33 mm and 0.12 mm, respectively.

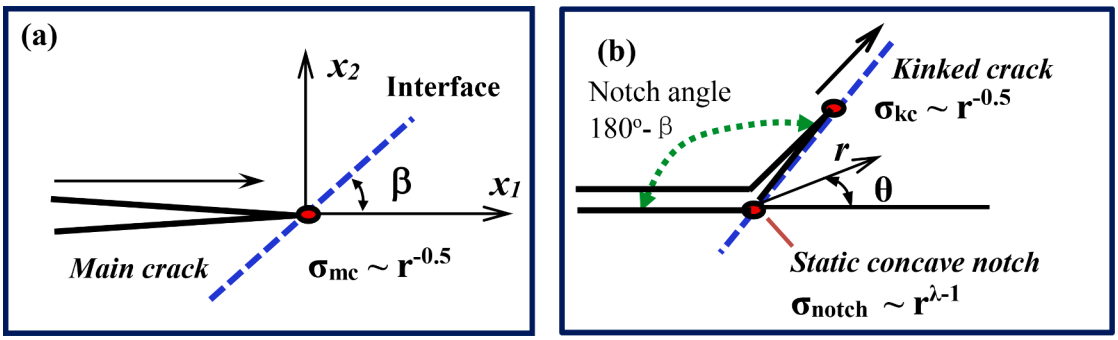

Fig. 3. (a) A main mode-I crack arrives and subsequently kinks at an interface with an interfacial angle β. A dark spot represents a crack or notch tip. (b) The interfacial crack kinks and leads to a sharp concave notch. The stress singular orders of the cracks and the notch are marked.

Table 1
Selected static and dynamic properties of Homalite.

Property	Different loading	
	Static (Strain rate ~ 10^{-3}/s)	Dynamic (Strain rate ~ 10^{3}/s)
Density ρ (kg/m^3)	1230	1230
Young's modulus (GPa)	3.45	3.45
Dilatational wave speed c_l (m/s) (plane stress)	1890	2119
Shear wave speed c_s (m/s)	1080	1208
Rayleigh wave speed c_R (m/s)	1010	1110
Poisson's Ratio ν	0.35	0.35
Material fringe constant fσ (kN/m)	23.7	23.7
Fracture toughness G_{IC} (J/m^2)	250	

Table 2
Selected material properties of PMMA.

Young's modulus (GPa)	3.5
Tensile strength (MPa)	75
Elongation (%)	4.5
Poisson's Ratio	0.35
Density (kg/m^3)	1410
Mode-I fracture toughness (MPa M$^{1/2}$)	2.13

process, whereas the CGS technique was used to record the gradient of the first in-plane stress invariant (fringes). To make an artificial interface, a rectangular polymer plate was cut into two parts that were bonded using two kinds of adhesives. A wedge was inserted into a pre-notch and when it was impacted by a projectile, the wedge opened the notch producing a single mode-I crack which was driven towards the inclined interface, as shown in Fig. 4. The projectile had a cylinder shape made of steel and plastic with a length of 58.1 mm and a diameter of 25.4 mm. Its weight was 0.0925 kg. Each specimen was in a free-standing position before impact. The initial crack length (notch length) was 12.7 mm. A high-speed camera (Cordin model 330A rotating mirror type, up to 2 million frames/second) was employed to record the entire failure process. Two identical specimens were made and tested for each impact case. Due to the difficulty of dynamic fracture experiments to obtain high-quality photos, only high-speed photos with better quality are shown in this paper. Because the experiment reported in this paper was an extension of our previously successful results [46], two identical specimens and tests still revealed the common fracture mechanics nature. Table 3 lists some special material properties, specimen sizes, and impact speeds for future modeling and simulation. These interfacial bonding strengths and fracture toughness were measured by Krishnan and Xu [18]. There is no standard definition of a strong or weak bonding/interface. The interfacial strengths and the mode-I fracture toughness of the adhesive W10 bonding were higher than those of the adhesive 384 bonding, so its bonding was considered "strong bonding." More experimental details were reported by Xu et al. [46]. Importantly, the high-speed photos published by Xu et al. [46] were different from the photos used in this paper because the current photos focused on the sharp notch effect, whereas the previous photos addressed crack kinking/penetration at the interface.

4. Results and discussion

4.1. Dynamic failure process of bonded Homalite plates

Fig. 4 shows a series of high-speed photos of the failure mode transition related to the strong interface of a bonded Homalite plate. The vertical line that appears in every image is the camera streak line, which was used for reference purposes. The slanted line in the figure indicates the position of the interface. The circular spot is a scaling mark, which was 6.35 mm in diameter.

Fig. 4(b) shows that a mode-I incident crack with a symmetrical fringe pattern/caustic approached a strong interface with an interfacial angle of 60°. The average model-I crack speed was around 400 m/s [46]. After the crack arrived at the interface, it became a mixed-mode interfacial crack with an unsymmetrical fringe pattern, as shown in Fig. 4(c) and (d). Therefore, a static concave notch of 120° formed between the incident crack and the kinked crack. Two caustics stemming from the static concave notch and the moving interfacial crack tip can be clearly seen in Fig. 4(d). If the interfacial strength was low and the same specimen was subjected to the same impact, the failure pattern became more complicated. Fig. 5 shows the new failure mode transition related to a weak interface of the same specimen. Initially, a large caustic was observed at the incident crack tip, as shown in Fig. 5(b). The time for the two incident cracks to arrive at the interfaces in Figs. 4(c) and 5(b) was very close. Similarly, a concave notch of 120° formed.

As shown in Fig. 5(c), one caustic appeared at the sharp notch, whereas the other moving caustic represented the kinked interfacial crack tip. As shown in Fig. 5(d), the distance between the two caustics increased because the sharp notch was static. The concave notch angle in Fig. 5(e) was approximately 120°, and its symmetric stress singularity order $(\lambda - 1) = -0.38$ [40], which was not small compared to −0.5 for a crack case with a notch angle of 0°. As shown in Fig. 5(e), the mixed-mode interfacial crack propagated after 20 mm and then kinked into the right side of the interface. Thus, a large caustic can be seen in Fig. 5(f). This indicates the mode-I nature of the second kinked crack, as predicted by previous researchers using mixed-mode fracture theory [10,48]. Similarly, the second concave notch formed between the interfacial crack and the second kinked crack. The notch angle was approximately 103°, as seen in Fig. 5(f), so a singular stress field existed.

4.2. Dynamic failure process of bonded PMMA plates

Even if the testing materials and optical techniques were different,

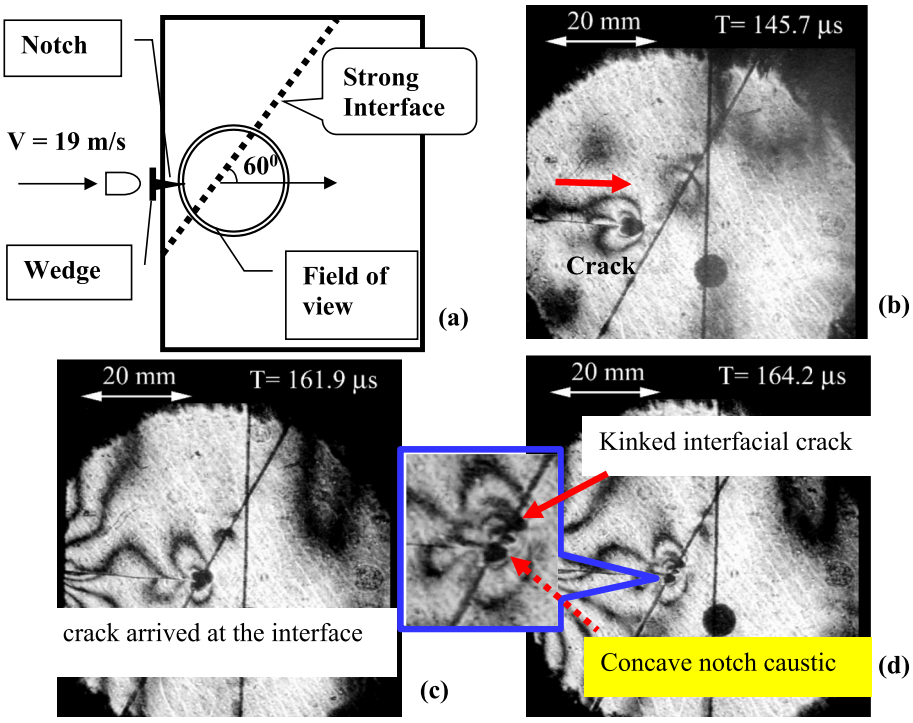

Fig. 4. High-speed photos showing crack kinking and one concave notch in a strongly bonded polymer specimen (code cdp60wd-1) after an incident mode-I crack arrived at the interface.

Table 3
Dynamic failure modes and sharp notch angles of different bonded materials.

Material/ bonding	Plate sizes (mm)	Impact speed (m/s)	Interfacial angle (degree)	Bonding normal strength (MPa)	Bonding shear strength (MPa)	Bonding toughness K_{IC} (MPa $m^{1/2}$)	Failure mode	Sharp notch
HM/W10 strong	457 * 254 * 10	19	60	7.74	21.65	0.83	Crack kinking	120°
HM/384 weak	457 * 254 * 10	17	60	6.75	7.47	0.38	Crack kinking and branching	120°& 103°
PMMA/W10 strong	508 * 381 * 10	46	60	20.87	21.35	1.74	Crack kinking, crack initiation from a notch	120°
PMMA/384 weak	508 * 381 * 10	40	45	12.66	11.58	0.71	Crack kinking	135°

the static notch phenomenon during dynamic crack kinking was still repeatable. Fig. 6 shows a series of CGS high-speed images of a PMMA plate with an interfacial angle of 45° and weak bonding. After an incident mode-I crack propagated toward the interface (120 μs), an interfacial crack propagated along the interface (140 μs). At 166 μs, a CGS fringe concentration appeared at the static concave notch formed between the incident and kinked interfacial cracks. This type of fringe concentration was not observed at 140 μs because of the low dynamic load acting on the notch.

Fig. 7 presents a large post-mortem photo of an impacted PMMA plate including four dynamic failure modes. The other photos are a series of CGS high-speed images that recorded the sequence and nature of these failure modes. At 52 μs after impact, an incident mode-I crack with a large caustic propagated towards the inclined interface. After this crack arrived at the interface at approximately 136 μs, an interfacial crack (failure mode #1) appeared and propagated along the interface at approximately 156 μs. The fringe pattern of the interfacial crack was not symmetric due to its mixed-mode nature. Additionally, a caustic was seen at the sharp concave notch formed between the incident crack and the kinked interfacial crack. After the interfacial crack propagated further along the interface (177 μs), the CGS fringes around the notch significantly expanded. So the effect of the concave notch should not be ignored. At the late stage (271 μs), a mode-I crack initiated from the sharp notch tip, and its initial crack path was very straight. The angle between this new mode-I crack and the interface was approximately 123°, as marked in the photo at 344 μs. Because the interface angle was 60°, the propagation direction of this mode-I crack stemming from the notch (failure mode #2) was almost in the middle of the concave notch (angle of 120°), which showed that the crack was caused by the high tensile stress acting at the notch tip.

Before 406 μs, this crack smoothly kinked (failure mode #3) because of its local load-mixity change (load-induced crack kinking), and finally changed its propagation direction by almost 90° (angle between the final crack propagation direction and the initial crack propagation direction, as seen in the large post-mortem photograph in Fig. 7). This curved crack path was carefully examined using a magnifying glass, and a lack of sharp kinking or sharp notches was found at every examination point. Simulation approaches, such as the extended finite element method (XFEM see [27]are often employed to simulate dynamic crack propagation paths. However, a largely curved crack path such as that recorded in this investigation has not previously been simulated because the current XFEM cannot simulate a largely curved crack path due to the limitation of its simple crack propagation criterion. For example, although the T-stress plays an important role in a crack path [8,5], it is not included in the XFEM software that is specialized in simulating crack paths. As previously stated in this paper, only some special fracture

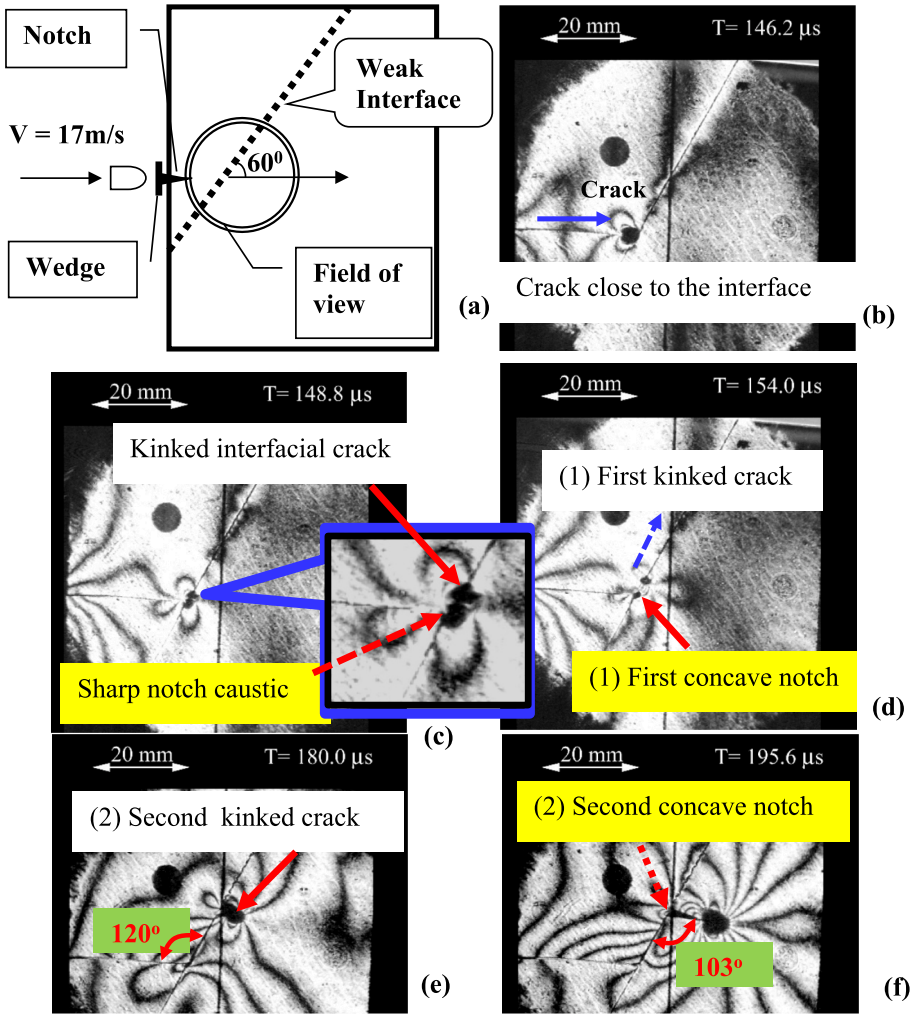

Fig. 5. Two dynamic crack kinking cases and two concave notches during impact failure of a weakly bonded polymer plate (specimen code cdp60i384-1), as recorded by a high-speed camera.

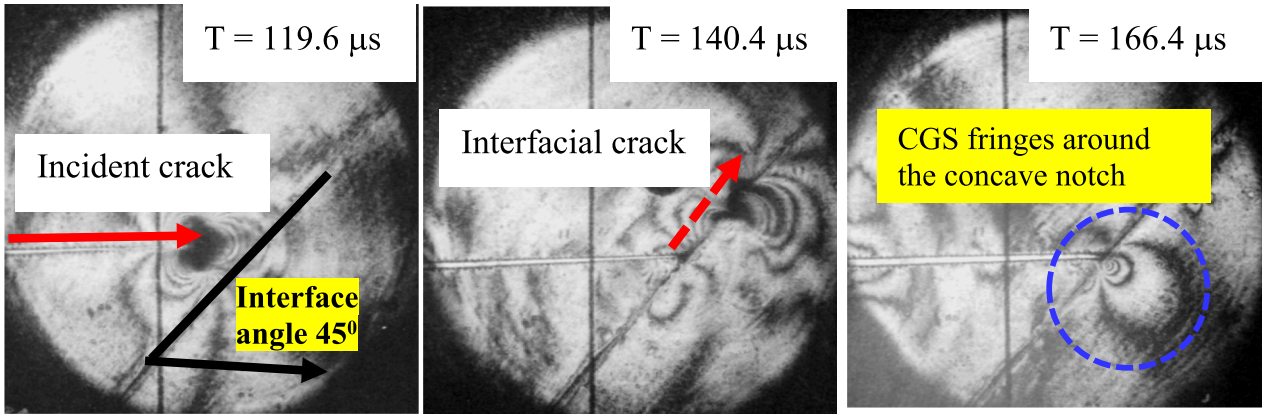

Fig. 6. High-speed photos of an impacted PMMA plate with weak interfacial bonding (impact speed 40 m/s, specimen code K45PM384-2). The incident crack (with a large caustic at the crack tip) arrived at the interface and kinked into the interface. A fringe concentration around the sharp notch was seen.

phenomena are reported to challenge the current modeling and simulation capabilities rather than proposing new modeling efforts by the author. Indeed, for most scientific research, modeling always occurs after the experimental phenomena.

The last failure mode (#4) was dynamic crack branching, which occurred much later and was not recorded by the high-speed camera. The notable result here was the angle between the two branched cracks (approximately 121°), which was much larger than 60°, i.e., the maximum theoretical crack branching angle [5]. Xu and Rosakis [44–46] reported that the experimental crack branching angle was slightly larger than the maximum crack branching angle. However, as shown in Fig. 7, the two branched cracks were arrested, whereas the

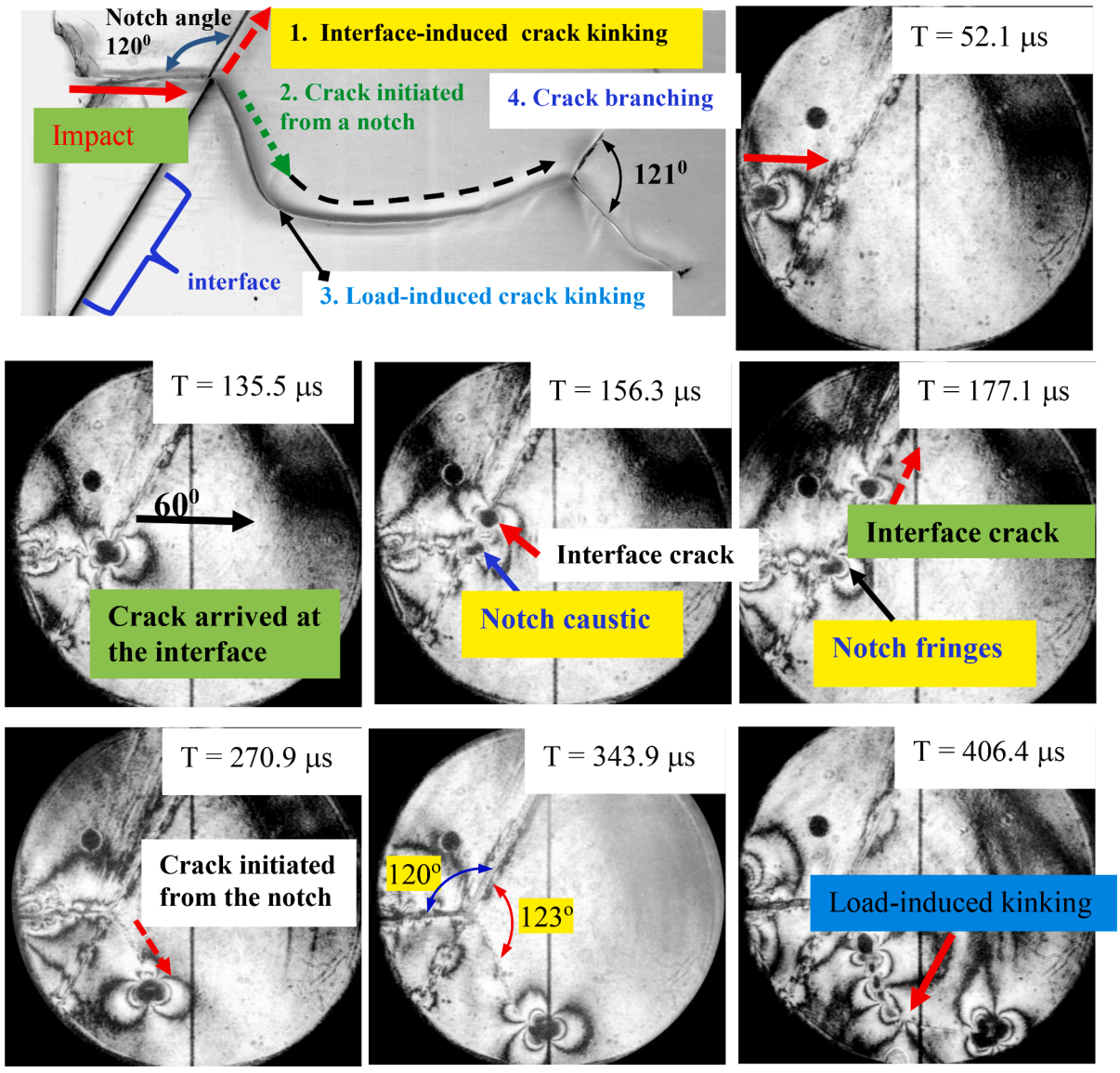

Fig. 7. Four major dynamic failure modes and their sequences of an impacted PMMA plate with strong interfacial bonding (interfacial angle 60°, impact speed 46 m/s, specimen code K60PMWD-1). A caustic at the static concave notch formed after dynamic crack kinking was seen around 156 μs. Then a crack initiated from this notch, smoothly kinked, and finally branched and arrested.

branched cracks in our previous experiment were not arrested. Evidently, a new criterion for dynamic crack branching is needed to understand this unique phenomenon, i.e., a very large crack branching angle and arrested branched cracks.

Based on the above experimental observations, the effect of the sharp concave notch should be considered during crack kinking modeling. If the singular stress field of a concave sharp notch is added to the right side of Eq. (2), an inequality will exist for two asymptotic stress fields before and after crack kinking:

$$\sigma_{ij}^{kc} \neq \sigma_{ij}^{mc} + \sigma_{ij}^{notch}\left(= K_I^{notch} r^{\lambda-1} f_{ij}(\theta) + K_{II}^{notch} r^{\xi-1} g_{ij}(\theta) \right) \quad (i,j = 1,2), \qquad (5)$$

because both σ_{ij}^{kc} and σ_{ij}^{mc} are functions of $r^{-0.5}$ or a constant stress singular order, whereas the notch stress singular orders are two functions of the notch angle. Therefore, it might not be possible to simply extend Contrell and Rice's assumption to analyze interface-induced crack kinking with a potential sharp notch. Further experimental evidence showed that the assumed "head-to-tail" crack kinking pattern might not hold.

4.3. *Interfacial crack nucleation and two convex notches without singular stresses*

An interfacial crack might have nucleated (event-1) before the incident crack arrived at the interface, as illustrated in Fig. 8(a), due to the high stresses ahead of the incident crack tip and the low interfacial strengths. When the incident crack reached the interface, the interfacial crack propagated away (event-2), as shown in Fig. 8(b). Notably, this interfacial crack had downward and upward tips. When the upward tip was moving, the downward tip might be arrested due to a small driven force (event-3). Fig. 8(c) shows that the Homalite-100 plate with weak interfacial bonding and an interfacial angle of 30° had two interfacial crack tips [46]. Some fast-moving fringes indicated the upward interfacial crack tip. However, very few fringes were observed at the downward tip, which was arrested, by examining other high-speed photos that are not shown here. We define this failure mode as the dynamic "Cook-Gordon mechanism." The static equivalent of this phenomenon was analyzed by Leguillon et al. [24]. Arata et al. [2] simulated further propagation of this type of interfacial crack with two different tips. Moreover, Wang and Xu [39] employed dynamic fracture mechanics

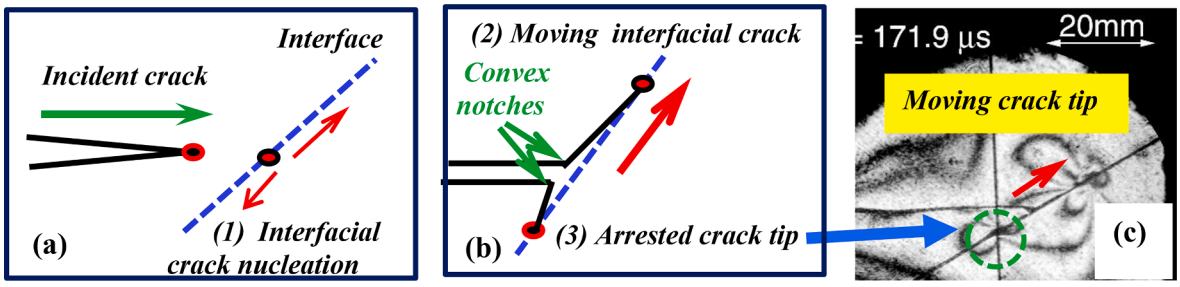

Fig. 8. (a) Before an incident crack arrives at the interface, an interfacial crack has nucleated. (b) After the incident crack arrives at the interface, the interfacial crack propagates away and leads to two sharp convex notches without singular stresses. (c) A high-speed photo supports this interfacial failure scenario. Click here to view a YouTube video based on high-speed photography.

theory and proposed a stress-based criterion to predict interfacial crack nucleation. In this interfacial failure scenario, two convex notches form. Because their notch angles are greater than 180°, the stresses at these notch tips are zero and will not be considered for modeling purposes.

We noticed a significant difference between the two types of crack kinking cases. The load-induced crack kinking, as shown in Fig. 7 (failure mode #3), had a very smooth crack path, and the local kinking angle was small at each point. No convex notch formed, as seen in the crack paths shown in Figs. 1 and 7. Cotterell and Rice [8] defined these cracks as "slightly curved or kinked cracks," although the final crack direction could be very large over a long crack path, as seen in Fig. 7. They derived Eq. (3) for small crack kinking angle cases, and the sharp concave notch effect was not considered. However, for interface-induced crack kinking, the interfacial failure scenarios are very complicated, and future new fracture mechanics models are expected to include the concave notch or the interfacial crack nucleation effect. It should be noted that some authors had simulated our previous experiments reported by Xu et al. [46], but none of them investigated the sharp notch effect [3,25,9].

5. Conclusion

High-speed photography of dynamic failure experiments of bonded polymers showed that different static notches formed if incident dynamic cracks arrived at material interfaces. In one scenario, the dynamic incident crack induced interfacial crack nucleation, and two convex notches formed after the interfacial crack propagated away. In another scenario, the dynamic incident crack might kink at the interface and the "head-to-tail" crack kinking pattern led to a concave notch, which had a singular stress field and should be considered in fracture mechanics modeling.

Declaration of competing interest

The authors declare that they have no known competing financial interests or personal relationships that could have appeared to influence the work reported in this paper.

Data availability

Data will be made available on request.

Acknowledgment

The author greatly appreciates the encouragement from Prof. Ares Rosakis at the California Institute of Technology.

References

[1] M.J. Alam, P. Parmigiani, J.J. Kruzic, An experimental assessment of methods to predict crack deflection at an interface, Eng. Fract. Mech. 181 (2017) 116–129.
[2] J.J.M. Arata, A. Needleman, K.S. Kumar, W.A. Curtin, Microcrack nucleation and growth in lamellar solids, Int. J. Fract. 105 (2000) 321–342.
[3] I.J. Arias, V.B. Knap, S.H. Chalivendra, M. Ortiz, A.J. Rosakis, Numerical modelling and experimental validation of dynamic fracture events along weak planes, Comput. Methods Appl. Mech. Eng. 196 (2007) 3833–3840.
[4] F. Arbeiter, M. Spoerk, J. Wiener, A. Gosch, G. Pinter, Fracture mechanical characterization and lifetime estimation of nearhomogeneous components produced by fused filament fabrication, Polym. Test. 66 (2018) 105–113.
[5] K.B. Broberg, Cracks and Fracture, Academic Press, San Diego, 1999.
[6] R.J. Cai, H.Q. Mao, Qu. Jia, Q. Guo, Experimental study of the quasi-static and dynamic fracture toughness of notched and repaired concrete using semi-circular bend method, Theor. Appl. Fract. Mech. 128 (2023) 104098.
[7] H.C. Chen, Q.L. Zhang, H. Chen, Z. Yang, Y. Wen, S. Hu, L. Chen, A two-set order parameters phase-field modeling of crack deflection/penetration in a heterogeneous microstructure, Comput. Methods Appl. Mech. Eng. 347 (2019) 1085.
[8] B. Cotterell, J.R. Rice, Slightly curved or kinked cracks, Int. J. Fract. 16 (1980) 155–169.
[9] I. Dooley, S. Mangala, L. Kale, P. Geubelle, Parallel simulations of dynamic fracture using extrinsic cohesive elements, J. Sci. Comput. 39 (2009) 144–165.
[10] F. Erdogan, G.C. Sih, On the crack extension in plates under plane loading and transverse shear, ASME J. Basic Eng. (1963) 519–527.
[11] L.B. Freund, Dynamic Fracture Mechanics, Cambridge University Press, New York, 1990.
[12] H. Gao, Y. Huang, P. Gumbsch, A.J. Rosakis, On radiation-free transonic motion of cracks and dislocations, J. Mech. Phys. Solids 47 (1999) 1941–1961.
[13] P.H. Geubelle, D. Kubair, Intersonic crack propagation in homogeneous media under shear-dominated loading: numerical analysis, J. Mech. Phys. Solids 49 (2001) 571–587.
[14] G.X. Gu, M. Takaffoli, A.J. Hsieh, M.J. Buehler, Biomimetic additive manufactured polymer composites for improved impact resistance, Extreme Mech. Lett. 9 (2016) 317–323.
[15] A.T. Gudmundsson, H. Simmenes, B. Larsen, S.L. Philipp, Effects of internal structure and local stresses on fracture propagation, deflection, and arrest in fault zones, J. Struct. Geol. 32 (2010) 1643–1655.
[16] J.W. Hutchinson, Z. Suo, Mixed mode cracking in layered materials, Adv. Appl. Mech. 29 (1992) 63–191.
[17] G. Hu, C.Q. Chen, K.T. Ramesh, J.W. McCauley, Mechanisms of dynamic deformation and dynamic failure in aluminum nitride, Acta Mater. 60 (2012) 3480–3490.
[18] A. Krishnan, L.R. Xu, Systematic evaluation of bonding strengths and fracture toughnesses of adhesive joints, J. Adhes. 87 (2011) 53–71.
[19] A.S. Kobayashi, S. Mall, Dynamic fracture toughness of Homalite-100, Exp. Mech. 18 (1978) 11–18.
[20] J. Kimberley, J. Lambros, Dynamic crack kinking from a PMMA/homalite interface, Exp. Mech. 44 (2004) 158–166.
[21] M. Lefranc, E. Bouchaud, Mode I fracture of a biopolymer gel: rate-dependent dissipation and large deformations disentangled, Extreme Mech. Lett. 1 (2014) 97–103.
[22] O.S. Lee, W.G. Knauss, Dynamic crack propagation along a weakly bonded plane in a polymer, Exp. Mech. 29 (1989) 342–345.
[23] L. Liu, Z. Ou, Z. Duan, A. Pi, F. Huang, Strain-rate effects on deflection/penetration of crack terminating perpendicular to bimaterial interface under dynamic loadings, Int. J. Fract. 167 (2011) 135–145.
[24] D. Leguillon, C. Lacroix, E. Martin, Interface debonding ahead of a primary crack, J. Mech. Phys. Solids 48 (2000) 2137–2161.
[25] J. Lei, Y.S. Wang, D. Gross, Numerical simulation of crack deflection and penetration at an interface in a bi-material under dynamic loading by time-domain boundary element method, Int. J. Fract. 149 (2008) 11–30.
[26] X.F. Li, L.R. Xu, T-stresses across static crack Kinking, ASME J. Appl. Mech. 74 (2007) 181–190.
[27] L. Moës, T. Belytschko, Extended finite element method for cohesive crack growth, Int. J. Numer. Meth. Eng. 46 (1999) 131–150.
[28] S.M.T. Mousavi, N. Richart, C. Wolff, J.F. Molinari, Dynamic crack propagation in a heterogeneous ceramic microstructure, insights from a cohesive model, Acta Mater. 88 (2015) 136–146.

[29] A. Needleman, A.J. Rosakis, The effect of bond strength and loading rate on the conditions governing the attainment of intersonic crack growth along interfaces, J. Mech. Phys. Solids 47 (1999) 2411–2449.
[30] H.V. Tippur, S. Krishnaswamy, A.J. Rosakis, A coherent gradient sensor for crack tip deformation measurements: analysis and experimental results, Int. J. Fract. 48 (1991) 193–204.
[31] N.D. Parab, W.W. Chen, Crack propagation through interfaces in a borosilicate glass and a glass ceramic, Appl. Glass Sci. 5 (2014) 353–362.
[32] K. Ravi-Chandar, W.G. Knauss, An experimental investigation into dynamic fracture. III. On steady state crack propagation and crack branching, Int. J. Fract. 26 (1984) 141–154.
[33] A.J. Rosakis, Two Optical Techniques Sensitive to Gradients of Optical Path Difference: The Method of Caustics and the Coherent Gradient Sensor (CGS), in: J. Epstein (Ed.), Experimental Techniques in Fracture, vol. III, 1992, pp. 125–170 (Chapter 5).
[34] A.J. Rosakis, O. Samudrala, D. Coker, Cracks faster than shear wave speed, Science 284 (1999) 1337–1340.
[35] Z.W. Shen, S.S. Liu, T. Ma, Modified F-criterion and its influence on potential crack deflection range, Int. J. Solids Struct. 160 (2019) 134–147.
[36] Ch. Song, F. Tin-Loi, W. Gao, A definition and evaluation procedure of generalized stress intensity factors at cracks and multi-material wedges, Eng. Fract. Mech. 77 (2010) 2316–2336.
[38] B.M. Sundaram, H.V. Tippur, Dynamic crack growth normal to an interface in bi-layered materials: an experimental study using digital gradient sensing technique, Exp. Mech. 56 (2016) 37–57.
[39] P. Wang, L.R. Xu, Dynamic interfacial debonding initiation induced by an incident crack, Int. J. Solids Struct. 43 (2006) 6535–6655.
[40] M.L. Williams, Stress singularities resulting from various boundary conditions in angular corners of plates in extension, J. Appl. Mech. 19 (1952) 526–528.
[41] P. Weißgraeber, W. Becker, Finite fracture mechanics model for mixed mode fracture in adhesive joints, Int. J. Solids Struct. 50 (2013) 2383–2394.
[42] D.A. Xie, KW.S. Waas, J.A. Schroeder, R.G. Boeman, Fracture criterion for kinking cracks in a tri-material adhesively bonded joint under mixed mode loading, Eng. Fract. Mech. 72 (2005) 2487–2504.
[43] J. Xie, D. Rittel, A two-dimensional model for metallic surface roughness resulting from pure waterjet peening, Int. J. Eng. Sci. 120 (2017) 189–198.
[44] L.R. Xu, A.J. Rosakis, An experimental study of impact-induced failure events in homogeneous layered materials using dynamic photoelasticity and high speed photography, Opt. Lasers Eng. 40 (2003) 263–288.
[45] L.R. Xu, A.J. Rosakis, Real-time experimental investigation of dynamic crack branching using high-speed optical diagnostics, SEM Exp. Tech. 27 (2003) 23–26.
[46] L.R. Xu, Y.Y. Huang, A.J. Rosakis, Dynamic crack deflection and penetration at interfaces in homogeneous materials: experimental studies and model predictions, J. Mech. Phys. Solids 51 (2003) 461–486.
[47] W. Yao, Y. Xu, K. Xia, et al., Dynamic mode II fracture toughness of rocks subjected to confining pressure, Rock Mech Rock Eng 53 (2020) 569–586.
[48] A.T. Zehnder, Fracture Mechanics, Springer, New York, 2012.
[49] X. Zeng, Y. Wei, Crack deflection in brittle media with heterogeneous interfaces and its application in shale fracking, J. Mech. Phys. Solids 101 (2017) 235–249.